ELSEVIER

Contents lists available at ScienceDirect

Chemical Physics Impact

journal homepage: www.sciencedirect.com/journal/chemical-physics-impact





Nonlinear optical behaviour of bis (cytosinium) tartarate monohydrate single crystal

P. Jaikumar^{a,*}, T. Balakrishnan^{b,*}, C. Indumathi^c, T.C. Sabari Girisun^d, K. Ramamurthi^e

- ^a PG & Research Department of Physics. National College (Autonomous). Affiliated to Bharathidasan University. Tiruchirappalli 620001. Tamil Nadu. India
- b Crystal Growth Laboratory, Department of Physics, Thanthai Periyar Government Arts and Science College (Autonomous), Affiliated to Bharathidasan University, Tiruchirappalli 620023, Tamil Nadu, India
- c PG and Research Department of Physics, Bishop Heber College (Autonomous), Affiliated to Bharathidasan University, Tiruchirappalli 620017, Tamil Nadu, India
- ^d Nanophotonics Laboratory, Department of Physics, Bharathidasan University, Tiruchirappalli 620024, Tamil Nadu, India
- ^e School of Physics, Bharathidasan University, Tiruchirappalli 620024, Tamil Nadu, India

ARTICLE INFO

Keywords: Single crystal XRD Thermal analysis Second harmonic generation Optical limiting Z-Scan

ABSTRACT

A nonlinear optical single crystal of bis (cytosinium) tartarate monohydrate (BCTM) was grown by slow evaporation method at room temperature. Single crystal X-ray diffraction study revealed their cell parameters and corresponding space group. Different functional groups were identified by using FTIR spectral analysis. Phase purity of the grown crystal was analysed by chemical etching and powder X-ray diffraction studies. The mechanical strength of the grown crystal was estimated using Vickers microhardness test. The thermal stability of the grown crystal was investigated by TGA-DTA studies. The optical absorption study was carried out in the wavelength range of 190–1100 nm. The dielectric response of the grown crystal was studied as a function of frequency at different temperatures. Second harmonic generation efficiency (SHG) was measured by Kurtz and Perry powder technique. The Z-scan pattern clearly evidenced that the BCTM exhibits sequential two photon absorption induced reverse saturable absorption.

1. Introduction

For the past few decades pyrimidine based derivatives have proved to be quiet effective in crystal engineering and pharmaceutical industry [1]. Among the four components of nucleic acids, cytosine (6-aminopyrimidine-2 one) is one of the naturally occurring pyrimidine bases found in deoxyribonucleic acid [2-3]. Due to the multiple complementary hydrogen bonding capability the cytosine plays a vital role in the area of biomolecular synthesis and biological applications [4-5]. The crystal structure of the hybrid compound formed by reaction of cytosine with oxalic acid was reported by Bouchouit et al. [6]. The hydrogen bonding in cytosinium dihydrogen phosphite was reported by Messai et al. [7]. Sridhar and Ravikumar [8] reported the multiple hydrogen bonds between cytosine and zoledronic acid. Molecular adducts of cytosine with COOH functional groups (benzoic acid, phthalic acid and isophthalic acid) were reported by Perumalla et al. [9]. The single crystal structure of cytosinium nitrate was reported by Cherouana et al. [10]. Sridhar and Ravikumar [11] studied the hydrogen bonded networks in cytosinium succinate and cytosinium 4-nitrobenzoate. The crystal structures of cytosine with nicotinic acid and isonicotinic acid were reported by Sridhar and Ravikumar [12]. Influence of anion substitution on hydrogen bonding patterns of cytosinium hydrogen sulfate and cytosinium perchlorate was reported by Bensegueni et al [13]. The synthesis, crystal growth, structural, physical, thermal and optical characterization of cytosinium hydrogen selenite [14] were reported for nonlinear optical applications. Our group synthesized the bis (cytosinium) tartarate monohydrate and grown the single crystal, solved the single crystal structure and reported the hydrogen bonding pattern of the crystal [15]. In continuation of our earlier reports, in the present work, we report on the growth of single crystals of bis (cytosinium) tartarate monohydrate along with different characterizations studies that include powder X-ray diffraction, Fourier transform infrared spectroscopy (FTIR), etching studies, thermal analysis, Vickers microhardness testing, dielectric evaluation, UV-vis-NIR transmittance and photoluminescence analysis. Further, the grown crystals were subjected to nonlinear optical characterization by powder second - harmonic generation (SHG) and Z-scan studies. Observation of SHG signal from bis (cytosinium) tartarate monohydrate crystals confirm the suitability of

E-mail addresses: jaiwinkumar@gmail.com (P. Jaikumar), balacrystalgrowth@gmail.com (T. Balakrishnan).

^{*} Corresponding authors.

Fig. 1. Scheme of Reaction for BCTM.

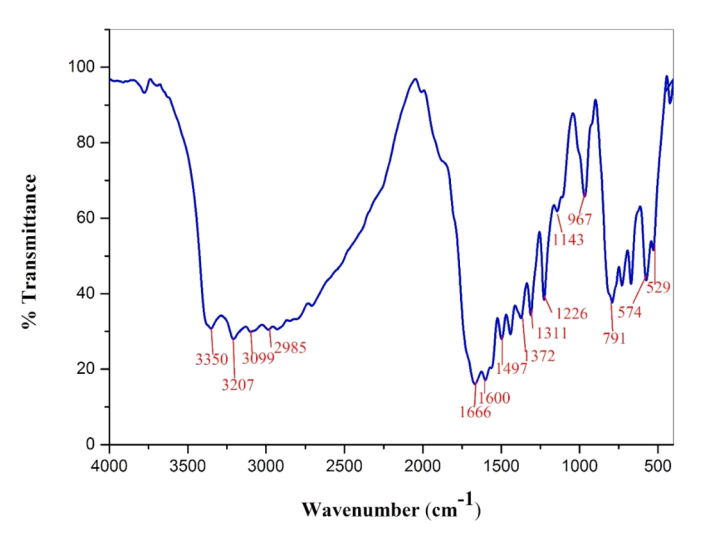


Fig. 2. FTIR spectrum of BCTM.

Table 1 FTIR band assignments for BCTM.

Wave number (cm ⁻¹)	Assignments	
3350	NH ₂ , asymmetric stretching vibration	
3207	NH ₂ , symmetric stretching vibration	
3099	NH asymmetric stretching vibration	
2985	NH symmetric stretching vibration	
1666	C=O stretching vibration	
1600	NH ₂ deformation	
1497	C—N—H stretching vibration	
1372	C=C stretching vibration	
1311	C-N stretching vibration	
1226	C-N stretching vibration	
1143	C—C—N asymmetric stretching	
967	CH ₂ rocking vibration	
791	C=O bending vibration	
574	COO - deformation	
529	COO rocking vibration	

the material for short-wavelength laser generation. Further the two-photon absorption induced optical limiting action and the potentiality of the material for laser safety devices are reported.

2. Synthesis and molecular confirmation

Cytosine (Merck-99%) and tartaric acid (AR grade-99%) taken in 1:1 molar ratio were used to prepare bis(cytosinium) tartarate monohydrate (BCTM) by simple acid-base reaction. Both materials were dissolved in double distilled water and the solution was stirred continuously for three hours using magnetic stirrer to obtain homogeneous mixture. Bis (cytosinium) tartarate monohydrate (BCTM) salt was obtained by evaporating the solvent and the reaction is shown in Fig. 1. The material

was purified by successive re-crystallization process using double distilled water.

To make a preliminary confirmation of the synthesized BCTM compound, the molecular structure was assessed by vibrational spectroscopy. FTIR spectrum of BCTM recorded in the wavelength range 400–4000 cm⁻¹ by employing Perkin Elmer FTIR spectrophotometer following the KBr pellet technique is shown in Fig. 2. The intense sharp peaks at 3350 cm⁻¹ and 3207 cm⁻¹ are due to NH₂ asymmetric and symmetric stretching vibrations of cytosine molecule respectively. Peaks due to N-H asymmetric and N-H symmetric stretching vibrations are observed at 3099 cm⁻¹ and 2985 cm⁻¹ respectively. The peak observed at 1666 cm⁻¹ is assigned to C=O stretching vibration of BCTM. The C—N —H stretching vibration is confirmed by the peak at 1497 cm⁻¹. The peak observed at 1372 cm⁻¹ is assigned to C=C stretching vibration. Absorption peak observed at 1311 cm⁻¹ is due to the C-N stretching vibration [16]. The asymmetric stretching vibration of C—C—N is observed at 1143 cm⁻¹. The intense peak observed at 967 cm⁻¹ and 791 cm⁻¹ are due to the CH₂ rocking and C=O bending vibrations respectively. The peak at 529 cm⁻¹ is assigned to COO⁻ rocking vibration. The observed wave number and tentative band assignments are presented in Table 1 and it confirmed the formation of desired molecular structure of BCTM.

3. Bulk growth, crystal structure and etching

The synthesized compound exhibits positive solubility gradient and the bulk growth of BCTM crystal was employed by solvent evaporation method. The supersaturated solution of recrystallized BCTM was prepared using double distilled water and filtered using whatman filter paper. The filtered solution was poured into crystallizing beaker. The crystallizing beaker kept at room temperature was closed with polythene and several holes were made on the polythene sheet. Beaker containing the solution was placed in a dust free environment and the slow solvent evaporation method was adopted. Evaporation of the solvent (water) yielded transparent platelets of BCTM crystals. Further we observed growth of some small size platelets of BCTM on the surface of the solution and these crystals settled - down at the bottom of the beaker in a few days. Transparent colourless platelets of BCTM crystals obtained in a growth period of about 12 days are shown in Fig. 3. One can observe the growth of small crystals on the surface of the BCTM crystals due to the secondary nucleation formed on the growing BCTM crystals.

Thin sheet like crystal morphology is one of the pre-requisite to utilize the material for laser applications like SHG device and optical limiter. Hence the grown crystals find the possibility to be tested for its SHG and optical limiting capability.

To determine the cell parameters, the grown crystal was subjected to single crystal X-ray diffraction study using Enraf Nonius CAD4 X-ray diffractometer with graphite monochromated Mo K α (λ = 0.71073 Å) radiation. The structure was solved with direct methods using SHELXS-97 [17] and refinement was done against F² using SHELXL – 97 [16]. The single crystal XRD analysis shows that bis (cytosinium) tartarate monohydrate single crystal belong to P2₁2₁2₁ non – centrosymmetric space group with orthorhombic crystal system having lattice parameter

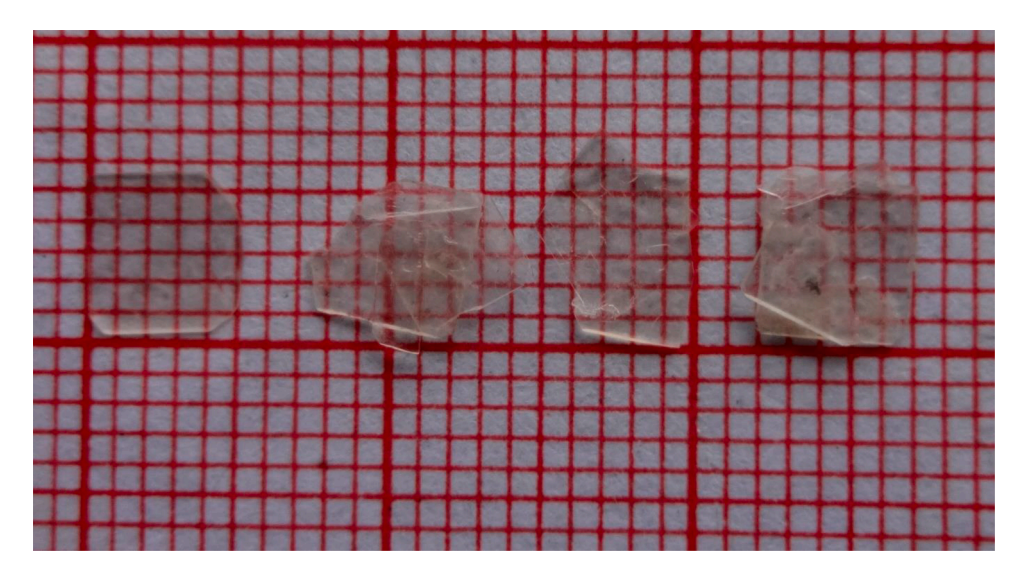


Fig. 3. Photograph of as grown BCTM crystals.

a=7.6932 (8) Å, b=10.1152 (8) Å and c=20.9336 (17) Å. [15]. Full crystallographic data (CIF file) relating to the crystal structure of BCTM has been deposited with the Cambridge Crystallographic Database (CCDC no. 1539281).

The symmetry of the crystal face and structural defects on the grown crystals was analysed using chemical etching study. The etching experiment was carried out on prominent face of as grown BCTM crystal for 5 and 10 s at room temperature. For both trails double distilled water was used as an etchant. At first, a transparent crack free crystal sample was selected and completely dipped in the etchant. After five seconds the etched sample was taken out and wiped using tissue paper. Etch patterns of BCTM were observed and photographed using high resolution optical microscope fitted with Motic camera in the reflected light mode. The microphotograph of BCTM before etching was shown in Fig. 4a. Before etching no particular etch pattern are visible on the surface. After etching with different etching time etch patterns were observed and etch pit morphology was changed. The photographs of etch patterns for 5s and 10 s are shown in Fig. 4b and c. Various dimensions of stacking lines were observed for 5 s. When the etching time is increased to 10 s etching lines became prominent and row of closely spaced pits are observed. During the etching process, a kind of periodical changes of etch pattern is observed in BCTM single crystal.

Powder X – ray diffraction pattern of the grown BCTM was recorded using BRUKER X - ray diffractometer with the Cu K α radiation ($\alpha=1.5406$ Å) in the range (20) of $10\text{--}80^\circ$ at the scanning rate of $1^\circ/\text{min}$. The recorded powder XRD pattern is shown in Fig. 5 and the observed peaks were indexed using XRD data analysis software to determine the phase purity of the crystal. The well-defined peaks and corresponding hkl planes of the powdered BCTM crystal are (004), (006) and (145). The sharp peaks found in the spectrum confirm the high degree of crystallinity.

4. Mechanical and thermal study

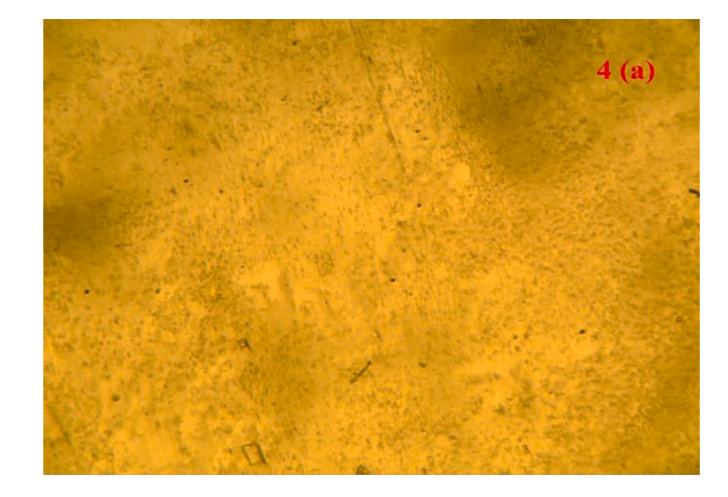
Microhardness test on the crystal is used to understand the relation between internal forces, deformation and external loads [18]. Among the available indentation hardness measurements, Vickers hardness study plays a vital role to understand the mechanical strength of the materials. Microhardness measurement was made on as grown bis (cytosinium) tartarate monohydrate crystal using HMV-2000 Shimadzu Vickers hardness tester fitted with an incident light microscope. A transparent crack free BCTM crystal with flat and smooth face is chosen for static indentation test. The selected face was indented gently by the loads varying from 5 to 100 g with the indentation time of 10 s. The

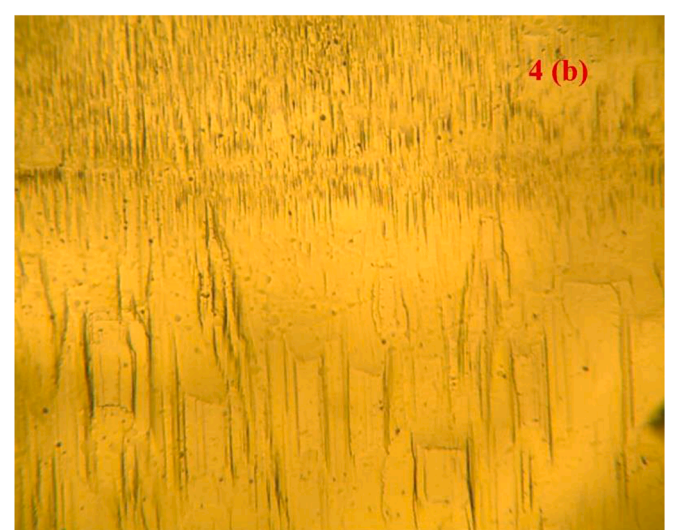
hardness values H_v were calculated using the relation $H_v=1.854\ P\ /\ d^2$, where P is the load applied in kg and d is the diagonal length of indentation mark in micrometres. The variation of H_v with applied load P for BCTM crystal is shown in Fig. 6. The variation of hardness number follows the reverse indentation size effect (RISE) i.e. H_v increases with increase in load upto 100 g. For the load above 100 g, several micro cracks were observed around the impression. The RISE was explained by Meyer's law, $P=k_1d^n$. Where k_1 is the material constant and n is the Meyer's index or work hardening coefficient. The work hardening coefficient was calculated from Fig. 7 by the least squares fit method. The n value for BCTM crystal is 2.25 and hence it belongs to soft material category [19,20]. Thus microhardness values ascertain the suitability of the grown crystals for NLO device fabrication.

Thermogravimetric analysis was carried out using NETZSCH STA 449F3 – Jupiter TGA unit under protected nitrogen purge, at a heating rate of 10 °C / min in the temperature range of 25–1200 °C. Sample of mass 7.201 mg was placed in the heating furnace to investigate the thermal behaviour. The thermogravimetric curve for BCTM is illustrated in Fig. 8. The sample is thermally stable upto 180 °C. Three stages of weight loss occurred in the compound. The first step of weight loss of about 5.08 % is due to loss of water molecules. Between 230 $^{\circ}\text{C}$ and 293 °C the second and major weight loss of 30.56% arose due to the decomposition of cytosine molecule. The final stage of weight loss of 45.89% is observed between 300 °C to 380 °C. In this stage of decomposition of tartaric acid molecule takes place. The final mass left out after the experiment is only 18.47% of the initial mass at a temperature of about 1000 $^{\circ}$ C. The differential scanning calorimetry (DSC) was also carried out in the temperature range 25-1200 °C with a heating rate of 10 °C / min in the nitrogen atmosphere. DSC trace is shown in Fig. 9. In DSC pattern, three endothermic peaks due to the decomposition of BCTM are observed at 188 $^{\circ}$ C, 226 $^{\circ}$ C and 292 $^{\circ}$ C and they coincide with the weight loss observed in thermogravimetry trace.

5. Linear optical properties: transmission, luminescence and dielectric studies

The optical transmission spectrum of bis (cytosinium) tartarate monohydrate single crystal was recorded in the wavelength region of 190–1100 nm using Varian Cary 5E spectrophotometer. Fig. 10 shows the UV–vis–NIR transmittance spectrum of BCTM recorded with optical quality single crystal of thickness 2 mm. The recorded transmittance spectrum shows that the BCTM crystal has a wide transparency window in the range from 320 nm to 1100 nm. The lower cut-off wavelength is observed at 200 nm. BCTM exhibits high linear transmittance in the





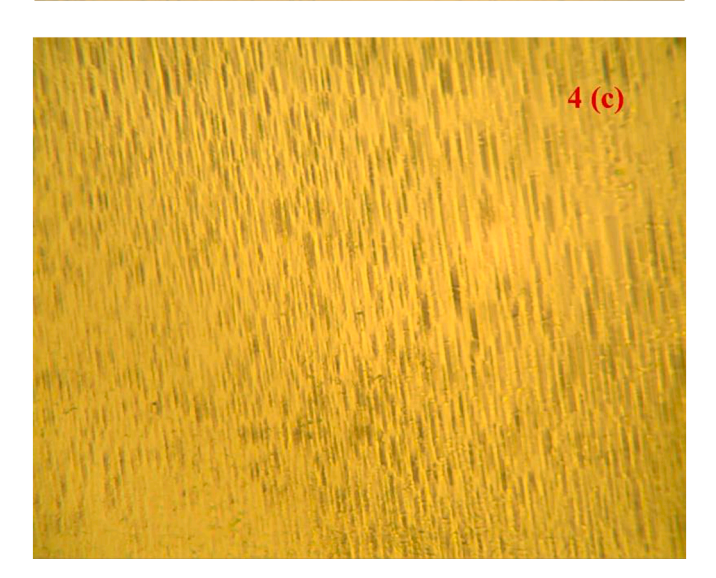


Fig. 4. Surface of as grown BCTM crystal (a) before etching, (b) etched for 5s and (c) etched for $10\ s$.

visible region and wide transparency window which are an essential criterion for NLO applications like SHG, OL (Optical limiting) devices. The absorption coefficient was evaluated from the transmittance data using the relation $\alpha=(1\ /\ t)$ log (1/T), where t is the thickness and T is the transmittance of the crystal. The direct band gap of the material was

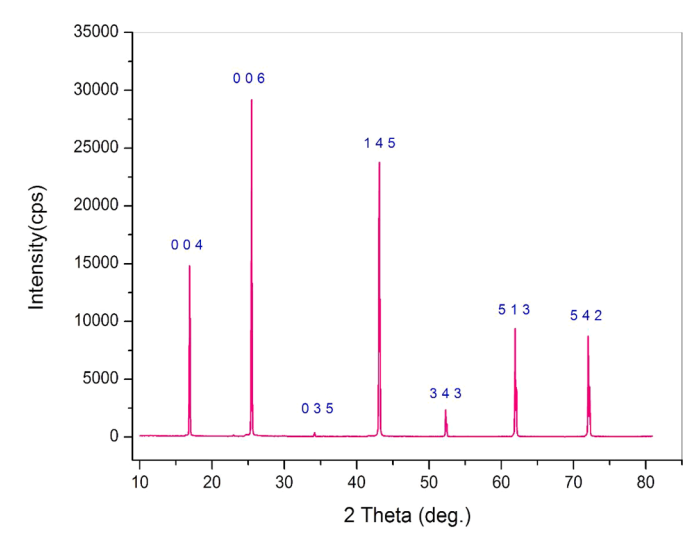


Fig. 5. Powder XRD pattern of BCTM crystal.

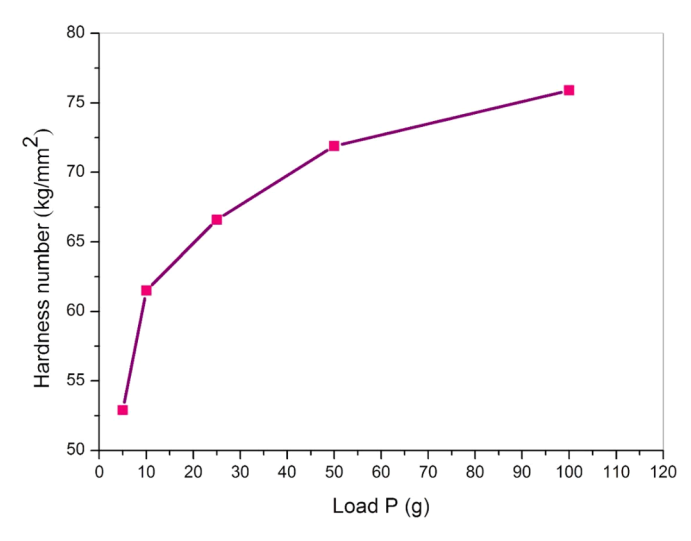


Fig. 6. Variation of Vickers hardness number with load for BCTM crystal.

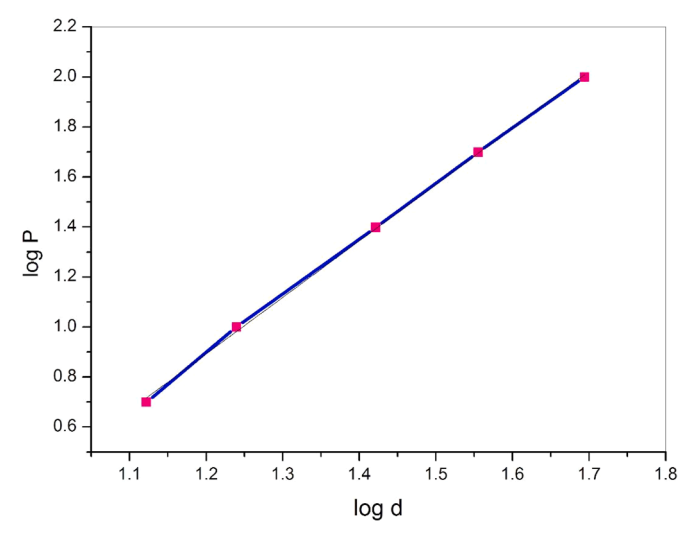


Fig. 7. Variation of log P against log d for BCTM crystal.

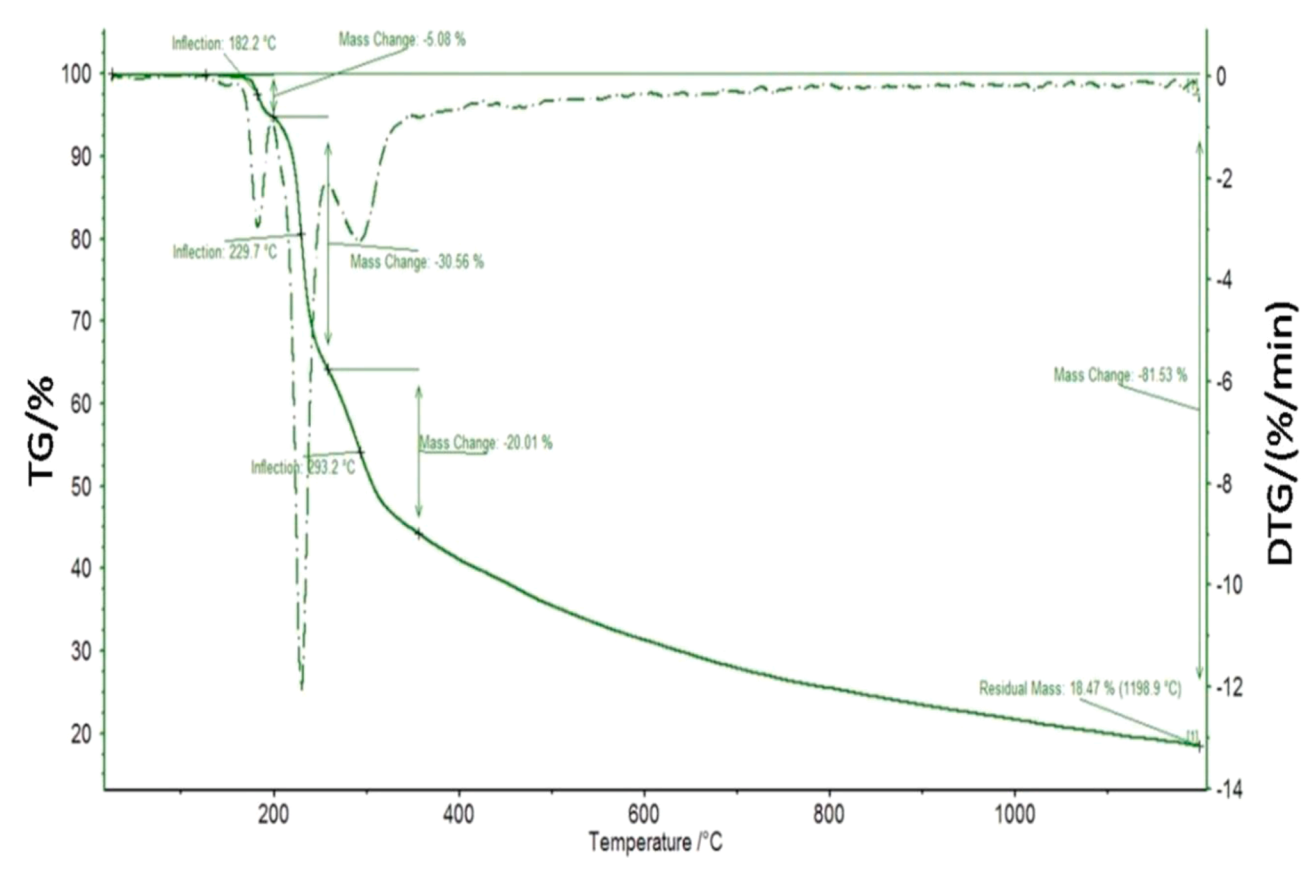


Fig. 8. TG / DTA analysis of BCTM crystal.

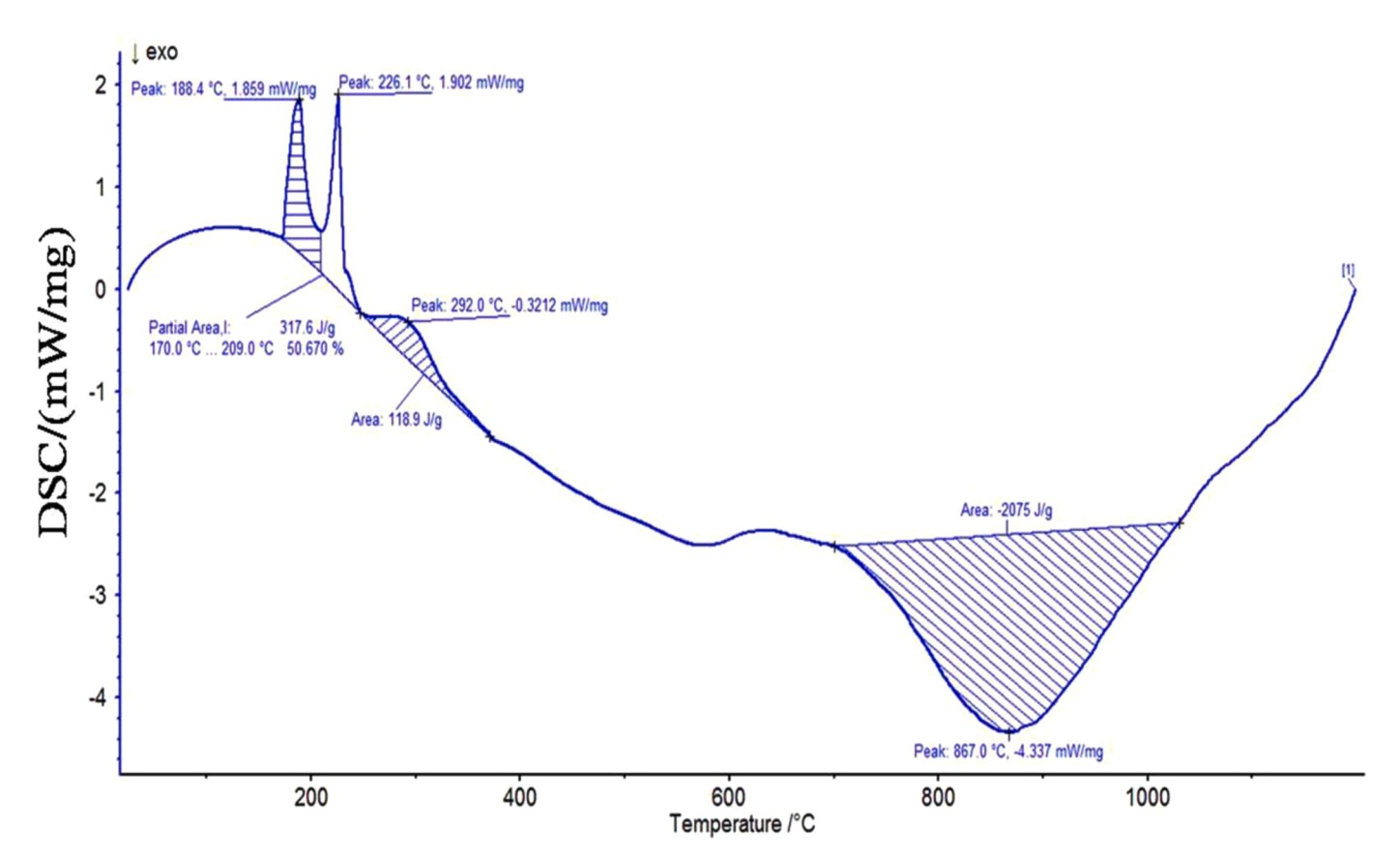


Fig. 9. DSC analysis of BCTM crystal.

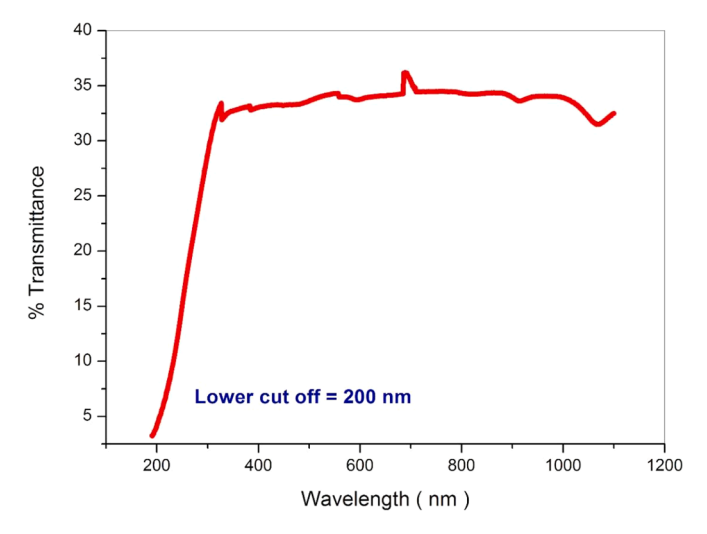


Fig. 10. Transmittance spectrum of BCTM single crystal.

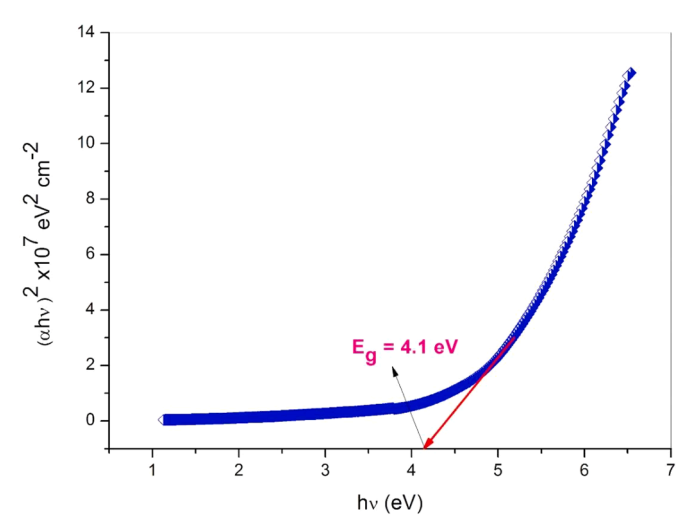


Fig. 11. Plot of $(\alpha h \nu)^2$ versus photon energy $(h \nu)$ for BCTM single crystal.

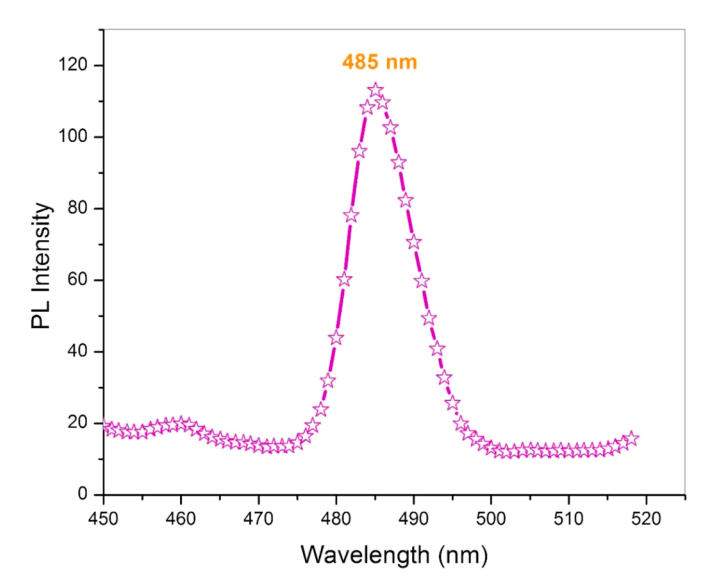


Fig. 12. Photoluminescence spectrum of BCTM single crystal.

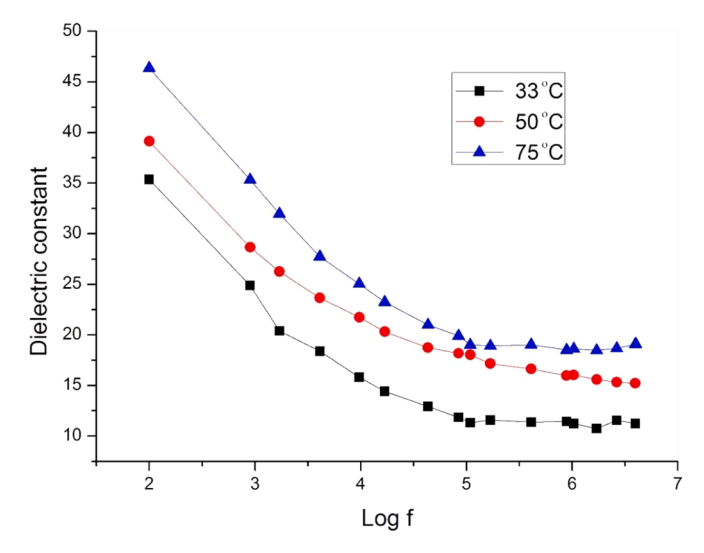


Fig. 13. Variation of dielectric constant with log frequency at various temperatures.

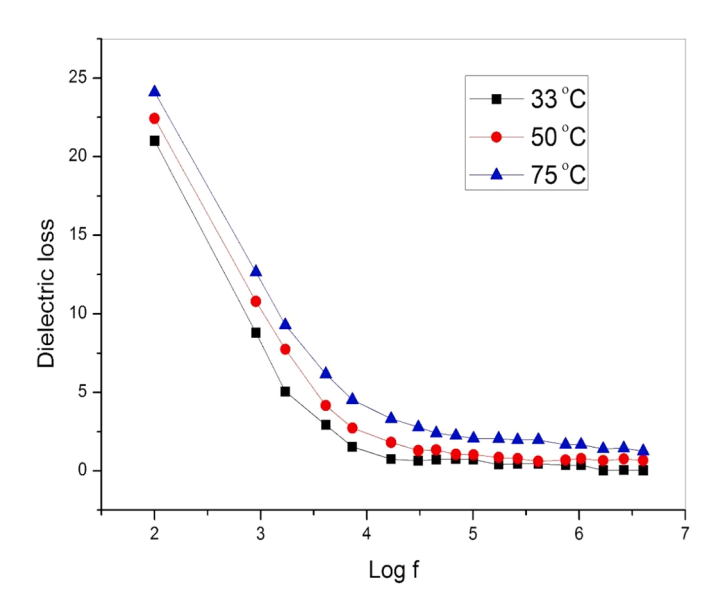


Fig. 14. Variation of dielectric loss with log frequency at various temperatures.

determined using the equation $ahv = A (hv - E_g)^{1/2}$, where E_g is the optical band gap of the material, hv is the photon energy and A is the constant related to material. A plot of variation of hv versus $(ahv)^2$ is shown in Fig. 11. Band gap energy was evaluated by extrapolating of the linear part with the energy axis [21] and the optical band gap energy of BCTM single crystal is found to be 4.14 eV. The wideband gap materials are suitable for two photon absorption process, when the materials are excited with green laser and thus BCTM can be used for fabricating optical limiting devices.

Photoluminescence (PL) studies are widely used in biochemical, medical and chemical research fields for analysing organic compounds. PL study finds important place in determination of crystal defects and the presence of impurities [22]. Crystal samples of BCTM were subjected to photoluminescence study at room temperature using Eclipse fluorescence spectrometer. The PL emission spectrum was recorded in the range of 290–520 nm at fluorescence mode. The excitation source wavelength of xenon arc lamp is 270 nm. The recorded spectrum with maximum intensity is shown in Fig. 12. A broad band was observed in the range of 470–500 nm with central maximum wavelength at 485 nm. Thus the result indicates that the BCTM crystals have the bright

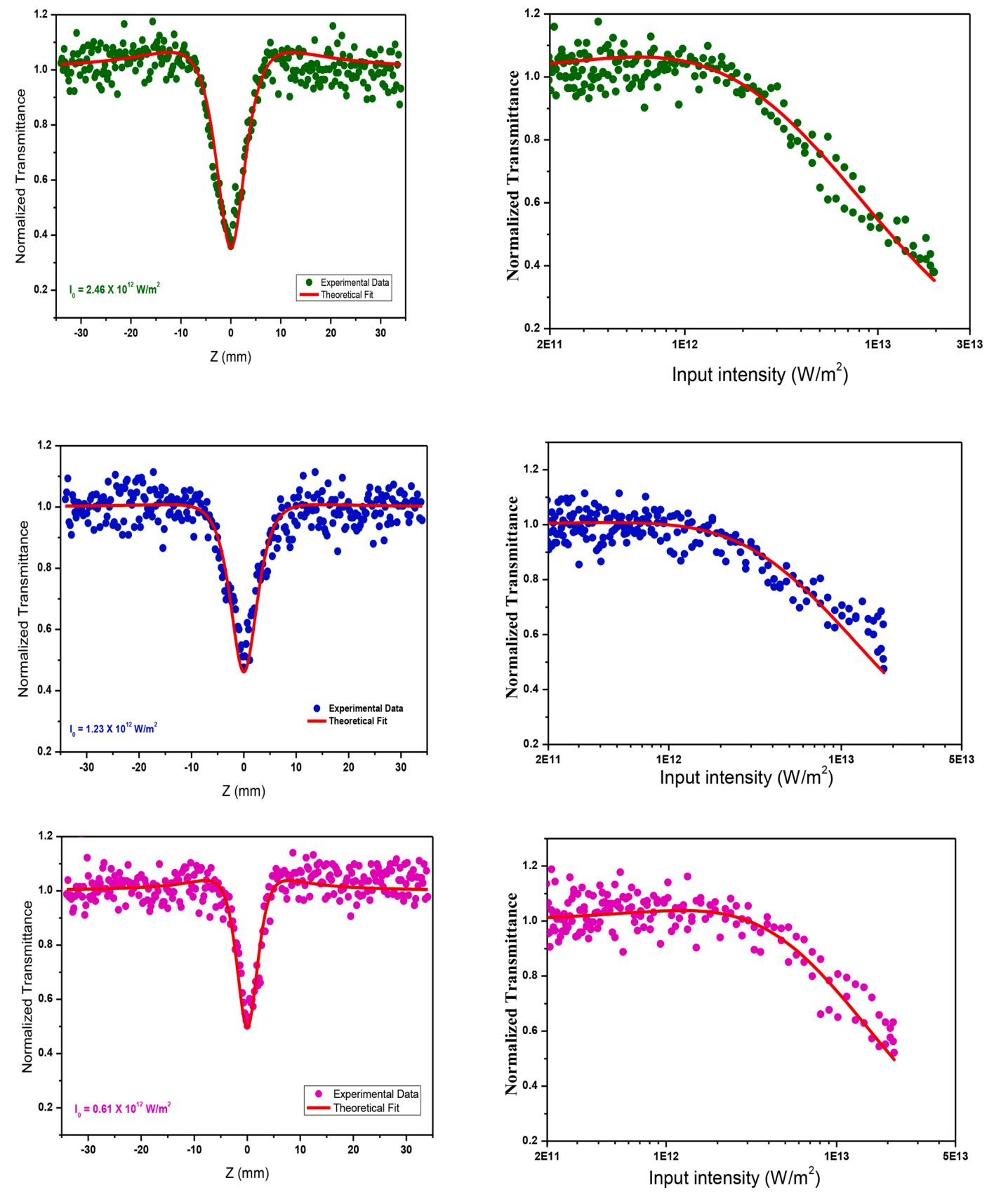


Fig. 15. OA Z-scan pattern and OL graph of BCTM at various on-axis peak intensities.

Table 2 Scan Data – Nd: YAG Laser (532 nm, 10 Hz, 9ns).

Sample Name	Intensity (\times 10^{12} W/m 2)	Nonlinear Absorption Coefficient ($\times~10^{-10}~\text{m}/$ W)	Optical Limiting Threshold ($\times~10^{12} \text{W/m}^2$)
BCTM	2.46	1.42	1.67
	1.23	1.04	2.45
	0.61	0.92	3.02

fluorescence emission in the visible region. From the maximum excitation wavelength the optical band gap was calculated using the relation. $E_g = (hc / \lambda e)$, where h is the Planck's constant, c is the velocity of light, e is the charge of an electron and λ is the maximum emission wavelength. The calculated optical band gap for BCTM single crystal is 2.6 eV and thus avails near-resonant energy state for excitation with green laser.

It is known that optical behaviour of a material is interrelated to its dielectric behaviour, especially for non - conducting medium [23]. The dielectric constant (ε_r) and dielectric loss (tan δ) were measured using multi frequency HIOKI 3536 LCR instrument in the frequency region from 100 Hz to 8 MHz. Grown crystal of dimensions $5 \times 4 \times 1 \text{ mm}^3$ was used for dielectric measurements. The sample was placed between two copper electrodes with silver coating on either sides to make it behave like a parallel plate capacitor. Capacitance and dielectric loss were measured for varying frequency values. The dielectric constant ϵ_{r} was calculated using the relation $\varepsilon_r = Cd/(\varepsilon_0 A)$ in which C is the capacitance, d is the thickness of the crystal, ε_0 is the vacuum dielectric constant and A is the area of the crystal. The variation of dielectric constant with frequency at three different temperatures (33, 50 and 75 °C) are shown in Fig. 13. It is found that dielectric constant decreases with increase in frequency followed by a frequency independent behaviour and the dielectric constant has high values in the lower frequency region [24]. The high value of dielectric constant at low frequencies is due to the presence of four such polarizations namely electronic, ionic, dipolar and space charge polarizations. The dielectric loss was calculated using the relation tan $\delta = \varepsilon_r D$, where D is the dissipation factor. Fig. 14 shows the variation of dielectric loss for different frequency points. As it can be seen from Fig. 15, the dielectric loss decreases rapidly with the increase of frequency. It is also indicated that the dielectric loss becomes high with raise in temperature. The higher values of dielectric loss at low frequency may due to the involvement of space charge polarization. The low value of dielectric constant and dielectric loss at high frequency

suggests that the BCTM crystal has good optical quality with lesser defects and it can be used for NLO applications.

6. Nonlinear optical properties: second harmonic generation and optical limiting

The second harmonic generation efficiency of BCTM was measured using the powder technique of Kurtz and Perry [25]. The NLO property was characterized by 8 ns pulse width Nd:YAG laser with a pulse repetition rate of 10 Hz working with fundamental wavelength at 1064 nm. The BCTM crystal was ground into fine powder and tightly packed in a capillary tube. The output from Nd: YAG laser with 6.1 mJ/pulse energy was used as source and it was passed through the sample after reflection from an IR reflector. The fundamental beam was filtered using IR filter and the green radiation of 532 nm was collected by photomultiplier tube (PMT-Philips photonics – model 8563). The output signal from the photomultiplier tube was converted into an electrical signal and displayed in CRO screen. A potassium dihydrogen phosphate (KDP) ground into samples of identical size was used as reference material in the SHG measurement. From the results the relative second harmonic generation efficiency of BCTM is found to be 0.9 times that of KDP.

Z-scan technique, a reliable method for determining the nonlinear optical properties of a material has been developed for identifying the materials for optical switching, polymerization and optical protection applications [26]. A frequency doubled, pulsed, Q-switched Nd:YAG laser operating at 532 nm was used to excite the prepared material. For nonlinear absorption measurements, open aperture Z-scan was performed with an input energy extending upto 100 µJ, at repetition rate of 10 Hz having pulse width of 9 ns. The experimental data were recorded without the aperture by monitoring the optical transmission as a function of sample position and input intensity along the incident beam. To avoid scattering issues, the grown crystal was cut and polished with extreme care to obtain optical quality crystal without any cracks and defects. Based on Sheik-Bahae [27] formalism, in order to treat the sample as thin media, the effective length of the sample (L) must be less than Rayleigh range (Z_R). So in typical experiment, a Gaussian beam was focused using a plano convex lens of focal length 200 mm upon the BCTM single crystal with thickness 1 mm (L < Z_R). The linear transmittance of the crystal was estimated to be 70%. The recorded open aperture Z-scan pattern and optical limiting graph is as shown in Fig. 15.

Nonlinear absorption coefficient, β was extracted from the best

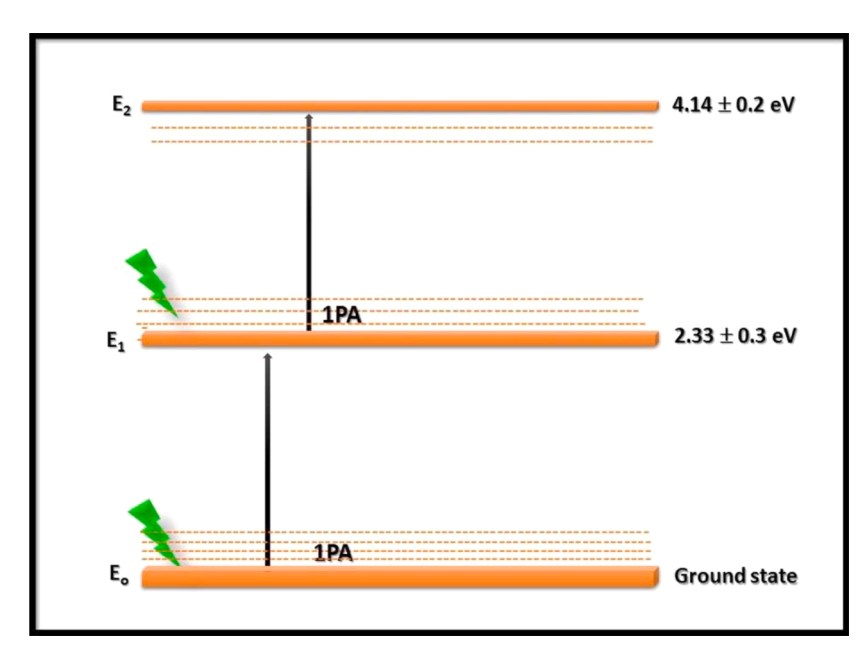


Fig. 16. Schematic representation of involved sequential 2PA process in BCTM.

theoretical fit generated on the basis of the below equation to the open aperture experimental data. The nonlinear absorption coefficient was obtained using the equation proposed by Sheik-Bahae et al. [27,28].

$$T(Z,S=1) \, = \left(rac{1}{\sqrt{\pi q_o(z,0)}}
ight) \int\limits_{-\infty}^{\infty} \, \ln(1+\,q_o(Z,0)e^{- au^2}) \,\, d au$$

Where, $q_o = \beta L_{eff} I_o$, I_o is the input laser intensity, L_{eff} is the effective length of the sample and β is the nonlinear absorption coefficient. In the fitted graph (Fig. 15), the circular spots represent the open aperture (OA) experimental data and the solid line corresponds to the theoretical fit generated for two photo absorption (2PA) using the equation. It can also be seen from the figure that the transmittance decreases as the magnitude of nonlinear absorption coefficient increases when the sample encounters higher intensity. It is clearly evidenced that the existence of positive nonlinearity resulted from 2PA induced reverse saturable absorption (RSA) in the sample. To confirm the nature of 2PA process, intensity dependent nonlinear absorption measurements were made and the values of 2PA coefficient of the prepared material (Table 2) were found to be increasing with on-axis intensity which clearly exposed the presence of sequential 2PA process. Fig. 16 infers the mechanism involved in sequential two photon absorption for BCTM. Generally, 2PA process occurs only when incident laser energy is greater than half of the bandgap of the sample. In the present case, the possible 2PA transition at 532 nm can be examined using the ground state absorption studies. From the absorbance and emission graph, it can be observed that a strong linear absorption takes place at 300 nm (4.41 eV) and the material avails emission state at 485 nm (2.56 eV) close to the excitation region 532 nm (2.33 eV). So, the involved 2PA transition is sequential where the electrons are transited from the ground state to the excited state at 532 nm (2.33 eV) by absorbing one photon and get trapped at the intermediate state. Soon after, this intermediate level promotes absorption of one more photon resulting in a sequential two photon absorption to excited state (300 nm, 4.41 eV).

Owing to the better RSA behaviour of the sample at 532 nm excitation, BCTM can be regarded as a suitable class of optical limiter i.e. the sample transmittance decreases as the input fluence increases (Fig. 15). As in the case of optical limiting measurement, the onset limiting threshold is an important parameter and it was determined from the corresponding open aperture Z-scan data. The position dependent fluence was evaluated from the equation

$$F(z) = \left[4\sqrt{\ln(2)} \ \left(\frac{E_{in}}{\pi^{\frac{3}{2}}}\right)\right] \bigg/ \ \omega(z)^2$$

where, F(Z) is the input fluence, E_{in} is the laser energy and $\omega(Z)$ is the radius of the laser beam at Z position [29]. The optical limiting performance of bis (cytosinium) tartrate monohydrate at 532 nm in pulsed regime exhibiting RSA behaviour is demonstrated in Fig. 15. Lower the limiting threshold better will be the optical limiting response and the intensity dependent limiting thresholds are listed in Table 2. Enhanced optical limiting behaviour observed for BCTM ($I_0 = 2.46 \times 10^{12} \,\mathrm{W/m^2}$) is due to the strong excited state absorption. Under Nd:YAG laser (532 nm, 9 ns) excitation, the estimated two-absorption coefficient of BCTM crystal was higher than other known 2PA materials such as 2-amino 5-nitropyridinium derivatives like 2A5NPBr (0.53 \times 10⁻¹⁰ m/W), 2A5NPDP (0.41 \times 10⁻¹⁰ m/W), 2A5NPCl (0.31 \times 10⁻¹⁰ m/W) [30,31], ethylenediaminium derivatives like EDA2NP (0.12 \times 10^{-10} m/W), EDA4NP (0.14 \times 10⁻¹⁰ m/W), EDA24DNP (0.79 \times 10⁻¹⁰ m/W) [32], thiopene dyes like HC (0.72 \times 10⁻¹⁰ m/W), DTBT (1.05 \times 10⁻¹⁰ m/W), PCTB (1.22 \times 10⁻¹⁰ m/W) [33], cadmium ferrite nanoparticles (0.29 \times 10^{-10} m/W), barium borate nanorods (0.17 × 10^{-10} m/W) [34,35], Gold: Graphene oxide composite (0.11 \times 10⁻¹⁰ m/W) [36] and most particularly benchmark materials like C^{60} (0.33 \times 10⁻¹⁰ m/W) [36]. The observations and results presented here, therefore, highlight the

possibility of utilizing this material in optical limiting applications.

7. Conclusion

Single crystal of bis (cytosinium) tartrate monohydrate a potential NLO single crystal was conveniently grown by slow solvent evaporation technique. The lattice parameters of the title compound elucitated by single crystal XRD confirms that the crystal belongs to the P2₁2₁2₁ noncentrosymmetric space group. The presence of various functional groups of BCTM was confirmed by Fourier transform infrared analysis. The thermogravimetric analysis reveals that the grown crystal is thermally stable in the region 25–180 $^{\circ}$ C. The Vickers microhardness study was conducted in order to understand the mechanical strength of the grown crystals. Etch figures are recorded by chemical etching technique which visualizes the regular growth features. Surface etching removes the unwanted micro crystals that are formed at the time of harvest. Optical absorption study showed that BCTM crystal is optically transparent over the entire region of visible region with band gap of 4.14 eV. The blue green PL fluorescent emission of 485 nm shows that the crystal might be promising for optoelectronic devices. The variation of dielectric constant and dielectric loss were studied with varying frequency at different temperature. The relative second harmonic efficiency (SHG) of BCTM is about 0.9 times that of KDP. Z-scan OA pattern clearly evidenced that the existence of positive nonlinearity resulted from 2PA induced reverse saturable absorption (RSA) in the sample. Intensity dependent Z-scan measurement and optical studies confirms that BCTM exhibit sequential 2PA process, ie., 1PA+ESA. Excited state absorption induced optical limiting action was demonstrated with 532 nm nanopulsed laser with onset limiting threshold of $1.67 \times 10^{12} \text{W/m}^2$. Thus it can be concluded that BCTM single crystals can be a utilized for the short wavelength laser generation by frequency doubling and laser safety devices by optical limiting action.

CRediT authorship contribution statement

P. Jaikumar: Conceptualization, Investigation, Writing – original draft. T. Balakrishnan: Project administration, Supervision. C. Indumathi: Conceptualization, Writing – original draft. T.C. Sabari Girisun: Project administration, Investigation, Supervision. K. Ramamurthi: Project administration.

Conflict of Interest

There is no conflict of interest.

Acknowledgments

The authors are thankful to Sophisticated Analytical Instrument Facility (SAIF), Indian Institute of Technology Madras, India for single crystal XRD analysis. The authors gratefully acknowledge Prof. P. K. Das, Department of Inorganic and Physical Chemistry, Indian Institute of Science, Bangalore for having extended the laser facilities for the SHG measurements.

References

- [1] A. Karthikeyan, R.S. Darious, P.T. Muthiah, F. Perdih, Supra-molecular hydrogen-bonding patterns in two cocrystals of the N(7)-H tautomeric form of N⁶-benzoyl-adenine: N⁶-benzoyl-adenine-3-hydroxy-pyridinium-2-carboxyl-ate(1/1) and N⁶-benzoyl-adenine-DL-tartaric acid (1/1), Acta. Cryst. C71 (2015) 985–990, https://doi.org/10.1107/S2053229615018094, 985–.
- [2] G. Portalone, M. Colapietro, Solid-phase molecular recognition of cytosine based on proton-transfer reaction, J. Chem. Crystallogr. 39 (2009) 193–200, https://doi. org/10.1007/s10870-008-9457-0.
- [3] B. Sridhar, J.B. Nanubolu, K. Ravikumar, Competition between the two-point and three-point synthon in cytosine–carboxylic acid complexes, J. Cryst. Eng. Comm. 14 (2012) 7065–7074, https://doi.org/10.1039/C2CE26076J.
- [4] G.M. Blackburn, M.J. Gait, Nucleic Acids in Chemistry and Biology, Oxford University Press, 1996.

- [5] E. Westhof, Formation of H adduct radicals in cytosine and Its derivatives, Int. J. Radiat. Biol. 23 (1973) 389–400, https://doi.org/10.1080/09553007314550441.
- [6] K. Bouchouit, N. Benali-Cherif, S. Dahaoui, E.E. Bendeif, C. Lecomte, Lecomte, Cytosinium oxalate monohydrate, Acta Cryst. E61 (2005) o2755–o2757, https://doi.org/10.1107/S1600536805023494.
- [7] A. Messai, N. Benali-Cherif, E. Jeanneau, D. Luneau, Hydrogen bonding in cytosinium dihydrogen phosphite, Acta Cryst. E65 (2009) o1147–o1148, https:// doi.org/10.1107/S1600536809014020.
- [8] B. Sridhar, K. Ravikumar, Multiple hydrogen bonds in cytosinium zoledronate trihydrate, Acta Cryst. C67 (2011) o115-o119, https://doi.org/10.1107/ S0108270111005191.
- [9] S.R. Perumalla, E. Suresh, V.R. Pedireddi, Nucleobases in molecular recognition: Molecular adducts of adenine and cytosine with COOH functional groups, J. Angew. Chem. 44 (2005) 7752–7757, https://doi.org/10.1002/anie.200502434.
- [10] A. Cherouana, K. Bouchouit, L. Bendjeddou, N. Benali-Cherif, Cytosinium nitrate, Acta Cryst. E59 (2003) o983–o985, https://doi.org/10.1107/ \$160053680301287X
- [11] B. Sridhar, K. Ravikumar, Supramolecular hydrogen-bonded networks in cytosinium succinate and cytosinium 4- nitrobenzoate cytosine monohydrate, Acta Cryst. C64 (2008) o566–o569, https://doi.org/10.1107/S010827010802979X.
- [12] B. Sridhar, K. Ravikumar, Supra-molecular hydrogen-bonded networks in cytosinium nicotinate monohydrate and cytosinium isonicotinate cytosine dihydrate, Acta Cryst. C66 (2010) o414–o417, https://doi.org/10.1107/ S0108270110026430
- [13] M.A. Bensegueni, A. Cherouana, L. Bendjeddou, C. Lecomte, S. Dahaoui, Influence of anion substitution on hydrogen-bonding patterns of salt compounds: Cytosinium hydrogen sulfate and cytosinium perchlorate, Acta Cryst. C65 (2009) o607–o611, https://doi.org/10.1107/S0108270109043765.
- [14] P. Jaikumar, S. Sathiskumar, T. Balakrishnan, K. Ramamurthi, Growth, structural, optical, thermal and mechanical properties of cytosinium hydrogen selenite: A novel optical single crystal, Mater. Res. Bull. 78 (2016) 96–102, https://doi.org/10.1016/j.materresbull.2016.02.019.
- [15] P. Jaikumar, T.V. Sundar, N. Sharmila, T. Balakrishnan, K. Ramamurthi, Hydrogen-bonding patterns in bis-(cytosinium) tartarate monohydrate, IUCrData 2 (×170448) (2017) 1–3, https://doi.org/10.1107/S2414314617004485.
- [16] K. Nakamoto, Infrared and Raman spectra of Inorganic and Coordination Compounds, Wiley, New York, 1978.
- [17] M. Sheldrick, SHELXL 97 crystal structure Refinement WinGX version, Copyright George (1993).
- [18] G.E. Dieter, Mechanical Metallurgy, McGraw Hill Education, India, 2013.
- [19] E.M. Onitsch, The present status of testing the hardness of materials, Mikroskopie 95 (1956) 12–14.
- [20] B.W. Mott, Micro Indentation Hardness Testing, Butterworths, London, 1956.
- [21] B.K. Periyasamy, R.S. Jebas, N. Gopalakrishnan, T. Balasubramanian, Development of NLO tunable band gap organic devices for optoelectronic applications, Mater. Lett. 61 (2007) 4246–4249, https://doi.org/10.1016/j.matlet.2007.01.105.
- [22] P. Mythili, T. Kanagasekaran, S. Stella Mary, D. Kanjilal, R. Gopalakrishnan, Swift heavy ion induced modification on the optical, mechanical and dielectric

- behaviour of GLS single crystals, Nucl. Instrum. Methods Phys. Res. Sect. B 266 (2008) 1737–1740, https://doi.org/10.1016/j.nimb.2007.11.065.
- [23] S.K. Arora, V. Patel, B. Amin, A. Kothari, Dielectric behaviour of strontium tartrate single crystals, Bull. Mater. Sci. 27 (2004) 141–147, https://doi.org/10.1007/ BE02708496
- [24] C.P. Smyth, Dielectric Behaviour and Structure, McGraw Hill, New York, 1995.
- [25] S.K. Kurtz, T.T. Perry, A powder technique for the evaluation of nonlinear optical materials, J. Appl. Phys. 39 (1968) 3798–3813, https://doi.org/10.1063/ 1.1656857.
- [26] S. Vadivel, AB. Sultan, SA. Samad, A. Shanmuganarayanan, R. Muthu, Synthesis, structural elucidation, thermal, mechanical, linear and nonlinear optical properties of hydrogen bonded organic single crystal guanidinium propionate for optoelectronic device application, Chem. Phys. Lett. 707 (2018) 165–171, https:// doi.org/10.1016/j.cplett.2018.07.055.
- [27] M. Sheik Bahae, A.A. Said, E.W. Van Stryland, High-sensitivity, single-beam n₂ measurements, Opt. Lett. 14 (1989) 955–957, https://doi.org/10.1364/ OL.14.000955
- [28] M. Sheik Bahae, A.A. Said, T.H Wei, D.J. Hagan, E.W. Van Stryland, Sensitive measurement of optical nonlinearities using a single beam, IEEE, J. Quant. Eletron. 26 (1990) 760–769, https://doi.org/10.1109/3.53394.
- [29] S. Dhanuskodi, T.C. Sabari Girisun, N. Smijesh, R. Philip, Two-photon absorption and optical limiting in tristhiourea cadmium sulphate, Chem. Phys. Lett. 486 (2010) 80–83, https://doi.org/10.1016/j.cplett.2009.12.069.
- [30] C. Indumathi, T.C. Sabari Girisun, Laser excitation dependent nonlinear absorption of 2-Amino 5-Nitropyridinium dihydrogen phosphate, Mol. Cryst. Liq. 692 (2019) 62–73, https://doi.org/10.1080/15421406.2019.1708028.
- [31] C. Indumathi, T.C. Sabari Girisun, Energy absorbing and energy spreading optical limiting action of 2-amino 5-nitropyridinium derivatives, Opt. Mater. 96 (2019) 109327–109334, https://doi.org/10.1016/j.optmat.2019.109327.
- [32] C. Indumathi, T.C. Sabari Girisun, G. Vinitha, S. Alfred Cecil Raj, Influence of number and position of nitro groups in tuning the thermodynamic and nonlinear optical properties of ethylenediaminium nitrophenolates, J. Mol. Liq. 238 (2017) 89–95, https://doi.org/10.1016/j.molliq.2017.04.115.
- [33] S. Anandan, S. Manoharan, N.K. Siji Narendran, T.C. Sabari Girisun, A.M. Asiri, Donor-acceptor substituted thiophene dyes for enhanced nonlinear optical limiting, Opt. Mater. 85 (2018) 18–25, https://doi.org/10.1016/j. optmat.2018.08.004.
- [34] G. Muruganandi, M. Saravanan, G. Vinitha, M.B. Jessie Raj, T.C. Sabari Girisun, Barium borate nanorod decorated reduced graphene oxide for optical power limiting applications, Opt. Mater. 75 (2018) 612–618, https://doi.org/10.1016/j. optics. 2017.11.017.
- [35] C Babeela, T.C. Sabari Girisun, Low temperature phase barium borate: A new optical limiter in continuous wave and nano pulsed regime, Opt. Mater. 49 (2015) 190–195, https://doi.org/10.1016/j.optmat.2015.09.018.
- [36] T.C. Sabari Girisun, M. Saravanan, V.R. Soma, Wavelength-dependent nonlinear optical absorption and broadband optical limiting in Au-Fe₂O₃-rGO nanocomposites, ACS, ACS Appl. Nano Mater. 11 (2018) 6337–6348, https://doi.org/10.1021/acsanm.8b01544.